Control Engineering Practice 174 (2026) 107019

Contents lists available at ScienceDirect

Control Engineering Practice

journal homepage: www.elsevier.com/locate/conengprac

Control-oriented nonlinear benchmark for floating offshore wind turbines with oscillating water column chambers: A WEC-Sim framework

Irfan Ahmad [a,*], Nataliia Sergiienko [b], Aitor J. Garrido [a], Izaskun Garrido [a]

[a] Automatic Control Group (ACG), Institute of Research and Development of Processes (IIDP), Department of Automatic Control and Systems Engineering, Faculty of Engineering of Bilbao, University of the Basque Country (UPV/EHU), Bilbao, Spain
[b] School of Electrical and Mechanical Engineering, University of Adelaide, Adelaide, South Australia, 5005, Australia

ARTICLE INFO

Keywords:
Floating offshore wind turbines
Control-oriented nonlinear modeling
Platform stabilization
WEC-Sim framework
Hybrid wind–wave systems

ABSTRACT

The design of advanced control strategies for floating offshore wind turbines (FOWTs) is limited by restricted access to platform motion states in widely used aero-hydro-servo-elastic simulation tools, where platform dynamics are embedded within servo modules and exposed through constrained interfaces. This limitation complicates closed-loop platform stabilization, particularly under high-wind and strongly coupled operating conditions. This paper presents a control-oriented nonlinear time-domain simulation framework that enables explicit platform pitch feedback and systematic analysis of controller-platform interactions.

The framework is implemented in MATLAB using WEC-Sim's multibody dynamics formulation and couples aerodynamic, hydrodynamic, mooring, and servo-dynamic subsystems within a unified time-domain model. The model is developed for the NREL 5-MW reference turbine mounted on an ITI Energy Barge platform incorporating an Oscillating Water Column (OWC) chamber. Platform geometry is defined in MultiSurf and processed hydrodynamics through WAMIT, while nonlinear mooring restoring forces are modeled using analytical catenary formulations. Nonlinear Froude-Krylov forces, viscous drag, quasi-static catenary mooring dynamics, and generator-converter dynamics are explicitly integrated, providing direct access to the full six-degree-of-freedom platform state vector throughout the simulation.

Model fidelity is assessed through free-decay tests, Response Amplitude Operator analysis (RAOs), and benchmark comparison against OpenFAST. The results demonstrate the accurate prediction of natural periods, resonance behavior, and operational responses, with close agreement in rotor torque, generator power, and platform pitch dynamics under combined wind-wave loading. By prioritizing control transparency over computational efficiency, the proposed framework provides a robust numerical foundation for feedback control synthesis, stability analysis, and robustness studies of floating wind-wave systems. The model establishes a verified baseline for the development of advanced platform stabilization strategies and hybrid control architectures in floating offshore wind turbines.

1. Introduction

Floating offshore wind turbines (FOWTs) have become a key enabling technology for wind-energy deployment in deep-water regions where fixed-bottom support structures are no longer technically or economically attractive (Aboutalebi et al., 2021). Rapid technological progress, cost reductions, and strong policy support are accelerating offshore deployment worldwide. The global offshore wind market is projected to grow substantially from 2024 to 2029, reflecting increasing investment and the expanding role of offshore renewables in future energy systems (Industry Research, 2024; Wind Energy Insights, 2024). This expansion is further supported by decarbonization targets and offshore renewable energy strategies in major markets, including the European Union and the United States (European Commission, 2023; U. S. Department of Energy, 2024; WindEurope, 2024). As shown in Fig. 1, the offshore wind sector is expected to experience sustained growth, reinforcing the need for advanced floating support technologies capable of operating reliably in deeper and more energetic marine environments.

At the same time, wave energy converters (WECs), particularly oscillating water columns (OWCs), are attracting increasing attention as complementary technologies for offshore renewable energy harvesting (Drew et al., 2009). Hybrid offshore systems that combine floating wind

* Corresponding author.
E-mail addresses: irfanahmad.irfan@ehu.eus (I. Ahmad), nataliia.sergiienko@adelaide.edu.au (N. Sergiienko), aitor.garrido@ehu.eus (A.J. Garrido), izaskun.garrido@ehu.eus (I. Garrido).

https://doi.org/10.1016/j.conengprac.2026.107019
Received 19 December 2025; Received in revised form 15 April 2026; Accepted 15 April 2026
Available online 25 April 2026
0967-0661/© 2026 The Author(s). Published by Elsevier Ltd. This is an open access article under the CC BY license (http://creativecommons.org/licenses/by/4.0/).

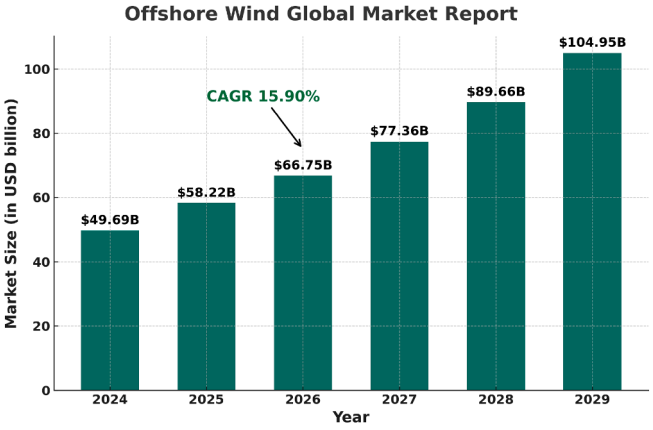

Fig. 1. Projected growth of the offshore wind market from 2024 to 2029.

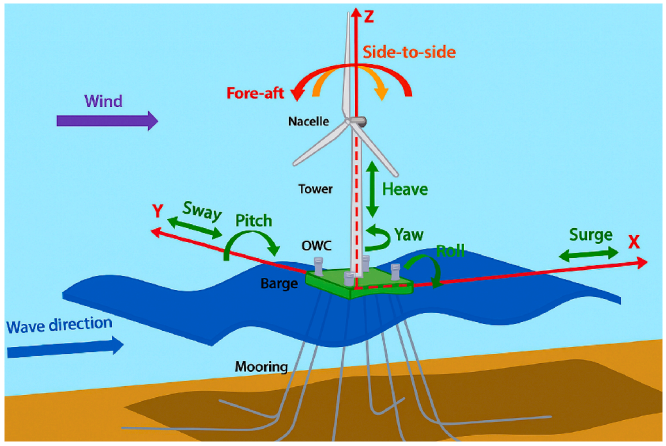

Fig. 2. Hybrid FOWT platform with OWcs integrated for active hydrodynamic damping, modeled using WEC-Sim.

and wave energy concepts are now recognized as an important research direction because they can exploit multiple marine resources while sharing structural and mooring infrastructure (Fu et al., 2019; Song et al., 2026). Among the available hybrid concepts, FOWT platforms integrated with OWCs are especially attractive because the OWC can act not only as an additional energy-conversion mechanism but also as a hydrodynamically influential subsystem that alters added mass, radiation damping, hydrostatic response, and wave excitation characteristics (Aboutalebi et al., 2021; Aubault et al., 2011; Chandrasekaran & Sricharan, 2021; Zhang et al., 2022). As a result, hybrid FOWT-OWC systems may offer improved energy capture, enhanced motion mitigation, and better overall platform performance. However, these advantages come with a substantially more challenging modeling and control problem due to the strong nonlinear coupling among aerodynamic, hydrodynamic, structural, mooring, and chamber-induced effects (Sarkar & Fitzgerald, 2020; Sergiienko et al., 2025). Fig. 2 shows the conceptual configuration of the hybrid FOWT-OWC platform considered in this work, together with the main platform motions relevant to coupled dynamic analysis and control-oriented modeling.

Existing studies have established important foundational insights into the hydrodynamic behavior and coupled responses of hybrid wind-wave systems. Early numerical and experimental work demonstrated the feasibility of integrating wave-energy concepts into floating wind platforms and showed that hybridization can influence both response amplitude and stability characteristics (Aubault et al., 2011; Chandrasekaran & Sricharan, 2021; Zhang et al., 2022). More recent studies have extended this line of research toward power performance, structural reliability, and integrated platform design. For example, offshore floating hybrid wind-wave converters have been analyzed in terms of array-dependent power performance and coupled response trends (Wei et al., 2025), while reliability assessment has been carried out for hybrid floating wind concepts using coupled aero-hydro-structural dynamics (Shittu et al., 2025). Additional hybrid configurations integrating floating offshore wind turbines with external WEC devices have also been proposed and evaluated through coupled time-domain simulations (Lin et al., 2025). Experimental and hybrid simulation studies further indicate that enhanced damping and active stabilization strategies can play an important role in suppressing platform oscillations under realistic environmental loading conditions (Xie et al., 2025; Zhai et al., 2025). Reported improvements such as pitch-motion reduction and higher energy capture continue to support the technical promise of hybrid floating platforms (Gu et al., 2025; Zhang et al., 2025). At the same time, the literature shows a clear shift toward more advanced control and control-oriented modeling for offshore renewable systems. Recent contributions include fuzzy-logic-based control for hybrid FOWT-OWC platforms (Ahmad et al., 2023a,b,c), intelligent vibration-control strategies and predictive stabilization methods (Bai et al., 2025; Fu et al., 2025; Hassan et al., 2025; He et al., 2025), machine-learning-assisted and AI-based prediction frameworks for platform motion (Ahmad et al., 2025; M'zoughi et al., 2018, 2020), and control developments targeting floating-turbine stabilization under coupled aerodynamic and hydrodynamic loading (Aboutalebi et al., 2026; Chen et al., 2024; Pereira et al., 2024; Rafia et al., 2026; Tang et al., 2026a; Wang et al., 2026). In addition, system-level numerical frameworks have recently been proposed for integrated wind-wave-to-wire simulation and offshore hybrid energy conversion (Yi et al., 2026). Collectively, these studies confirm that the field is moving beyond feasibility assessment toward integrated, data-informed, and control-aware offshore renewable energy modeling.

A structured comparison of representative studies is provided in Table 1, where the existing literature is organized according to modeling focus, control strategy, and limitations from a control-design perspective. The comparison shows that much of the available work falls into one of three categories: hydrodynamic and performance analysis without explicit controller synthesis, controller development based on reduced-order or surrogate representations, or coupled simulation studies that are not formulated for transparent access to the full set of nonlinear platform states and interaction forces. Although these studies have significantly advanced the understanding of hybrid offshore systems, they also reveal that a fully nonlinear and control-oriented benchmark framework with direct state accessibility is still limited.

This gap is particularly important for platform-level feedback control. High-fidelity aero-hydro-servo-elastic tools are well established for load analysis, verification, and performance assessment of FOWTs. However, comparatively fewer studies have focused on nonlinear benchmark models that are explicitly structured for control synthesis, stability analysis, and real-time interaction with platform dynamics. In practical terms, a benchmark model intended for advanced control design should preserve the essential nonlinear behavior of the floating platform under large motions while also providing direct and synchronous access to coupled subsystem states, hydrodynamic loads, mooring reactions, and controller input-output channels.

OpenFAST is widely used for coupled FOWT simulation and certification studies because of its modular treatment of aerodynamic, hydrodynamic, structural, and control subsystems. Nevertheless, its DLL-based control architecture is primarily designed for conventional turbine-control workflows. While highly effective for many engineering applications, this structure can restrict direct access to internal platform states and typically applies control actions at a prescribed servo rate that is not fully synchronized with all underlying nonlinear dynamic interactions. For platform-level feedback design, especially in hybrid FOWT-OWC systems, these limitations can reduce transparency and complicate controller development based on directly available physical states.

Table 1
Representative literature on nonlinear modeling, coupled analysis, and control of floating offshore wind turbines and hybrid FOWT-OWC / wind-wave systems.

Reference	Modeling / Control Focus	Limitations for Control Design
Zhang et al. (2022) (Zhang et al., 2022)	Coupled modeling of hybrid FOWT-OWC platforms with focus on feasibility and hydrodynamic interactions.	No feedback control design; limited analysis of controller-platform interaction.
Aboutalebi et al. (2021) (Aboutalebi et al., 2021)	Dynamic performance analysis of barge-type FOWT-OWC systems with emphasis on stability metrics.	OWC treated as a passive element; no closed-loop platform control.
Ahmad et al. (2023) (Ahmad et al., 2023a)	Fuzzy-logic control for hybrid FOWT-OWC configurations.	Based on reduced-order models; limited representation of nonlinear coupling.
Sebastian et al. (2024) (Sebastian et al., 2024)	Time-domain simulation of semi-submersible FOWTs with OWCs using WEC-Sim.	Response-focused; platform states not structured for control synthesis.
Wei et al. (2025) Wei et al. (2025)	Power performance of offshore hybrid wind-wave converters under varying configurations.	Focus on energy capture; no platform-level feedback control.
Shittu et al. (2025) (Shittu et al., 2025)	Reliability assessment using coupled aero-hydro-structural modeling.	Emphasis on reliability; not formulated for control design.
Lin et al. (2025) (Lin et al., 2025)	Design and performance evaluation of hybrid FOWT platforms with WEC integration.	Limited direct access to nonlinear states for feedback control.
Ahmad et al. (2025) (Ahmad et al., 2025)	AI-based framework for real-time prediction of platform pitch.	Prediction-oriented; not a physics-based control benchmark.
Wang et al. (2026) (Wang et al., 2026)	Model predictive control of auxiliary stabilizers for FOWTs.	Uses simplified state-space models; limited hydrodynamic detail.
Tang et al. (2026) (Tang et al., 2026b)	State-space modeling and control for wet towing operations.	Operational focus; not applicable to in-situ stabilization.
Rafia et al. (2026) (Rafia et al., 2026)	Neural-network-based adaptive control for FOWT operation.	Validated within conventional frameworks with limited state access.
Aboutalebi et al. (2026) (Aboutalebi et al., 2026)	Dynamic stabilization of hybrid FOWT-OWC platforms.	Implementation remains solver-dependent.
Song et al. (2026) (Song et al., 2026)	Review of hybrid offshore wind-wave systems and integration strategies.	Review only; no control-oriented benchmark model.
Yi et al. (2026) (Yi et al., 2026)	Coupled framework for wind-wave-to-wire energy conversion.	System-level focus; lacks explicit feedback control formulation.
Tang et al. (2026b) (Tang et al., 2026a)	Individual pitch control for coupled platform-rotor dynamics.	Restricted access to full platform-state variables.
Aslmostafa et al. (2026) (Aslmostafa et al., 2026)	Experimental validation of robust nonlinear controllers for FOWTs.	Not integrated with high-fidelity nonlinear hybrid platform models.
This work	**Fully nonlinear, control-oriented time-domain model of a hybrid FOWT-OWC platform with direct access to 6-DOF states and coupling forces in MATLAB/Simulink.**	**Enables direct synthesis and validation of platform feedback controllers beyond DLL-based limitations.**

To address these limitations, this work develops a *control-enabling simulation architecture* for a hybrid FOWT-OWC platform based on the multibody dynamics formulation of WEC-Sim within a unified MATLAB/Simulink environment. The objective is not simply to reproduce coupled offshore renewable energy dynamics, but to provide a nonlinear benchmark model that preserves the essential aero-hydro-mooring-servo interactions while exposing the variables needed for direct controller synthesis and validation. In the proposed framework, aerodynamic loading, hydrodynamic radiation and excitation forces, hydrostatics, mooring restoring loads, and drivetrain-servo dynamics are integrated within a single nonlinear time-domain formulation.

Hydrodynamic coefficients are obtained from WAMIT for the ITI Energy Barge geometry developed in MultiSurf, and a quasi-static catenary mooring model is adopted to capture nonlinear restoring behavior during large platform excursions. The framework provides synchronous access to the full six-degree-of-freedom platform state vector together with the principal nonlinear force contributions at each integration step, thereby enabling direct implementation of multi-variable platform feedback strategies. The OWC chamber is incorporated at the geometric and hydrodynamic levels, where it acts as an integrated moonpool that modifies mass distribution, hydrostatic stiffness, added mass, radiation damping, and wave excitation loads through multi-body hydrodynamic interaction. Although active OWC damping and power take-off dynamics are beyond the scope of the present study, the proposed architecture remains modular and can accommodate these subsystems in future developments.

The main contribution of this paper is therefore a fully nonlinear, control-oriented benchmark model for hybrid FOWT-OWC platforms that enables direct synthesis and validation of platform feedback controllers without the state-access limitations commonly encountered in conventional DLL-based workflows. By bridging the gap between high-fidelity offshore renewable energy simulation and controller-oriented nonlinear modeling, the proposed framework is intended to support advanced stabilization studies and future developments in hybrid offshore wind-wave energy systems.

The remainder of this paper is organized as follows. Section 2 describes the modeling methodology and numerical implementation. Section 3 presents verification results, including free-decay tests, response amplitude operator analysis, and benchmark comparison with OpenFAST. Section 4 investigates system response under combined wind-wave excitation and demonstrates platform pitch feedback control. Section 5 summarizes the main findings and outlines directions for future research on active stabilization and hybrid energy extraction.

2. Methods and tools

In this study, various advanced tools were utilized to model the hydrodynamic, structural, and mooring behavior of the floating barge equipped with OWCs and a wind turbine. The integrated analysis approach leverages time-domain, frequency-domain, and quasi-static simulations to evaluate the platform's dynamic performance under wind-wave forces. The following key modeling tools were employed: WECSim, WAMIT, MOST, and MATLAB/Simulink. Each tool serves a specific function in capturing the intricate interactions between waves, the structure, and mooring forces.

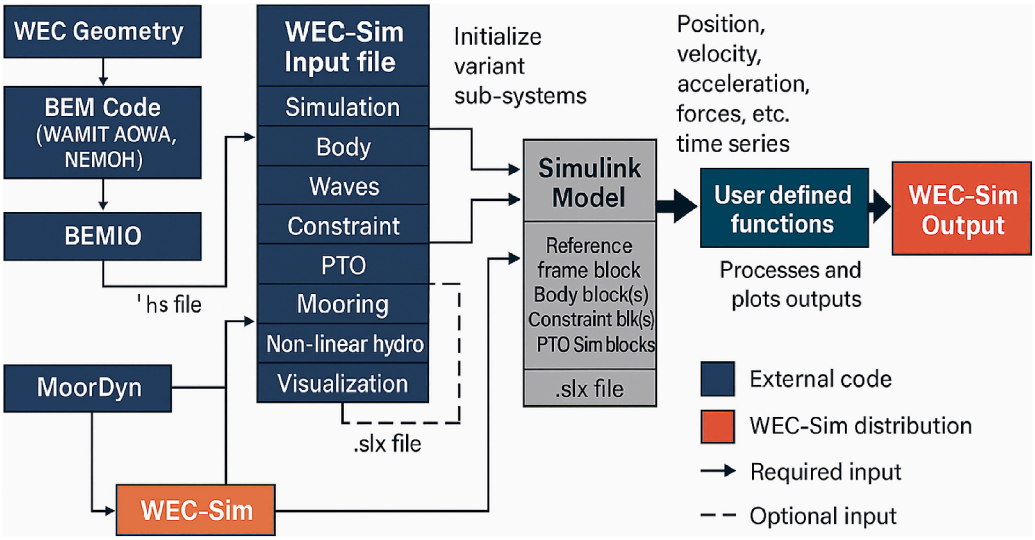

Fig. 3. WEC-Sim process flow chart illustrating the workflow from Boundary Element Method (BEM) code input to time-domain simulation and output generation. External BEM tools provide hydrodynamic data that WEC-Sim uses to simulate device performance in MATLAB/Simulink.

2.1. Wave energy converter SIMulator-WECsim

In this study, WEC-Sim was used to simulate the hydrodynamic performance of a floating barge equipped with an OWC chamber under real sea conditions. The platform's dynamic response, including motion in 6-DOF (surge, sway, heave, roll, pitch, and yaw), energy absorption from waves, and interaction with mooring lines, was evaluated. Additionally, WEC-Sim facilitated an analysis of different control strategies to optimize the energy extraction from the OWCs.

Fig. 3 provides an overview of the WEC-Sim workflow, starting from BEM code generation of hydrodynamic data, passing through WEC-Sim's input file structure, and ending with the time-domain simulation in Simulink. The output includes time series data such as body position, velocity, forces, and PTO performance, which are further processed using user-defined functions for custom analysis and visualization. The sinusoidal steady-state formulation assumes the platform response mirrors the periodic nature of the incoming wave and is therefore limited to regular wave scenarios. Under this assumption, the radiation force is calculated as a function of the platform's velocity and acceleration using frequency-dependent added mass and radiation damping matrices:

$$\mathbf{F}_{\text{rad}}(t) = -\mathbf{A}(\omega)\ddot{\mathbf{X}} - \mathbf{B}(\omega)\dot{\mathbf{X}}, \tag{1}$$

where $\ddot{\mathbf{X}}$ and $\dot{\mathbf{X}}$ are the body acceleration and velocity vectors, $\mathbf{A}(\omega)$ is the added mass matrix, and $\mathbf{B}(\omega)$ is the radiation damping matrix, both dependent on the wave frequency ω. The incoming wave field is represented using linear wave theory, assuming monochromatic wave components defined by their height, frequency, and water depth. The resulting wave excitation force is given by:

$$\mathbf{F}_{\text{exc}}(t) = \Re\left[R_f(t)\frac{H}{2}\mathbf{F}_{\text{exc}}(\omega,\theta)e^{i\omega t}\right], \tag{2}$$

where $\Re$ denotes the real part, $R_f(t)$ is a time-dependent ramp function to avoid transients, H is the wave height, $\mathbf{F}_{\text{exc}}$ is the complex frequency-domain excitation force amplitude, and θ is the incident wave angle.

The time-averaged second-order mean drift force originates from two primary physical effects: the nonlinear pressure contributions generated by the wave field itself, and the interactions between first-order wave-induced body motions and the incident wave excitation. In WEC-Sim, only the first contribution is currently modeled using pre-computed mean drift coefficients, if available from the BEM input files. The resulting time-domain mean drift force is computed as:

$$F_{\text{md}}(t) = \left(\frac{H}{2}\right)^2 F_{\text{md}}(\omega,\theta), \tag{3}$$

and is added to the excitation force in the output response signal provided by the solver.

An approximation will need to be made as the convolution kernel K_r is solved from a set of partial differential equations, whereas a linear state space is constructed from a set of ordinary differential equations. In general, a linear system is desired such that:

$$\dot{X}_r(t) = \mathbf{A_r}X_r(t) + \mathbf{B_r}\mathbf{u}(t); \quad X_r(0) = 0$$
$$\int_0^t \mathbf{K_r}(t-\tau)d\tau \approx \mathbf{C_r}X_r(t) + \mathbf{D_r}\mathbf{u}(t) \tag{4}$$

with $\mathbf{A_r}$, $\mathbf{B_r}$, $\mathbf{C_r}$, $\mathbf{D_r}$ being the time-invariant state, input, output and feed-through matrices, while u is the input to the system and X_r is the state vector describing the convolution kernel as time progresses.

2.1.1. Calculation of K_r from state-Space matrices

Consider a linear time-invariant (LTI) system represented in state-space form with a single input and zero initial conditions. The system dynamics can be expressed as:

$$\dot{x} = \mathbf{A_r}x + \mathbf{B_r}u, \tag{5}$$
$$y = \mathbf{C_r}x, \tag{6}$$

where u represents an impulse input. Assuming the system starts at zero state, the impulse response corresponds to the evolution of the state from the initial condition $x(0) = \mathbf{B_r}u$, and with no input thereafter ($u = 0$), the system reduces to:

$$\dot{x} = \mathbf{A_r}x, \tag{7}$$
$$y = \mathbf{C_r}x. \tag{8}$$

This formulation yields the zero-state response of the system. For systems with a non-zero feedthrough term ($\mathbf{D_r} \neq 0$), the impulse response is not finite at $t = 0$. Therefore, the value $\mathbf{C_r}\mathbf{B_r}$ is typically reported as the limiting value at that instant to maintain continuity.

The general solution for the system state over time is given by:

$$x(t) = e^{\mathbf{A_r}t}x(0) + \int_0^t e^{\mathbf{A_r}(t-\tau)}\mathbf{B_r}u(\tau)\,d\tau, \tag{9}$$

where $e^{\mathbf{A_r}t}$ denotes the matrix exponential. Using this, the time-domain expression for the system's impulse response kernel $K_r(t)$ is defined as:

$$K_r(t) = \mathbf{C_r}e^{\mathbf{A_r}t}\mathbf{B_r}. \tag{10}$$

In time-domain hydrodynamic modeling, state-space realization provides a compact and computationally efficient representation of the radiation force kernel. The objective is to identify a minimal-order discrete-time system that approximates the radiation impulse response, using the associated state-space matrices $\mathbf{A_d}$, $\mathbf{B_d}$, $\mathbf{C_d}$, $\mathbf{D_d}$ derived from sampled data.

This task is typically easier in the discrete-time domain due to the straightforward interpretation of the impulse response as a sequence of Markov parameters, expressed as:

$$\tilde{\mathbf{K}}_r(t_k) = \mathbf{C_d}\mathbf{A_d}^k\mathbf{B_d}, \tag{11}$$

where $t_k = k\Delta t$ for $k = 0, 1, 2, \ldots$ and Δt is the sampling interval. To ensure causality and avoid singular behavior at $t = 0$, the feedthrough matrix $\mathbf{D_d}$ is generally set to zero.

One widely adopted method for obtaining the system realization is through the application of Singular Value Decomposition (SVD) to the Hankel matrix formed from the impulse response sequence, as introduced by Kung (Kung et al., 1983). The state-space order and system matrices are inferred from the dominant singular values and the corresponding decomposition.

The structure of the Hankel matrix H based on the impulse response is given by:

$$H = \begin{bmatrix} \mathbf{K_r}(2) & \mathbf{K_r}(3) & \cdots & \mathbf{K_r}(n) \\ \mathbf{K_r}(3) & \mathbf{K_r}(4) & \cdots & 0 \\ \vdots & \vdots & \ddots & \vdots \\ \mathbf{K_r}(n) & 0 & \cdots & 0 \end{bmatrix} \tag{12}$$

Analysis of the singular values of H often shows that only a limited number of states significantly contribute to the system dynamics. Therefore, a reduced-order model can be constructed by retaining only the dominant modes, resulting in an accurate yet efficient state-space representation.

2.1.2. Waves interactions and power

Regular (or monochromatic) waves are idealized as two-dimensional sinusoidal surface elevations propagating uniformly in space and time. The free surface elevation $\eta(x, y, t)$ at a given location and time is expressed as:

$$\eta(x, y, t) = \frac{H}{2}\cos\left(\omega t - k(x\cos\theta + y\sin\theta) + \phi\right), \tag{13}$$

where H is the wave height, ω is the angular frequency ($\omega = 2\pi/T$), k is the wave number ($k = 2\pi/\lambda$), θ is the wave heading angle, and ϕ is the phase shift. This formulation assumes planar wave fronts with constant amplitude and period, typically used for validation and steady-state hydrodynamic response analysis.

The average power transmitted by a regular wave per unit crest length is governed by both wave amplitude and propagation characteristics. This power flux, P_w, can be determined using:

$$P_w = \frac{1}{2}\rho g A^2 c_g, \tag{14}$$

where ρ is the water density, g is the gravitational constant, $A = H/2$ is the wave amplitude, and c_g is the group velocity, which describes the speed at which energy travels through a wave train.

The group velocity in intermediate and deep water is derived from wave dispersion relations and is given by:

$$c_g = \frac{\partial\omega}{\partial k} = \frac{1}{2}\sqrt{\frac{g}{k}\tanh(kh)}\left(1 + \frac{2kh}{\sinh(2kh)}\right), \tag{15}$$

where h is the water depth, and sinh denotes the hyperbolic sine function. The first term inside the expression corresponds to the wave phase velocity, c_p.

Using this relation, wave power can be expressed as:

$$P_w = \frac{1}{4}\rho g A^2\sqrt{\frac{g}{k}\tanh(kh)}\left(1 + \frac{2kh}{\sinh(2kh)}\right). \tag{16}$$

This expression can be further simplified in the limiting cases of deep and shallow water:

$$P_w \approx \begin{cases} \frac{1}{4}\rho g A^2\sqrt{\frac{g}{k}} = \frac{1}{8\pi}\rho g^2 A^2 T, & \text{for } kh \gg 1 \\ \frac{1}{4}\rho g A^2\sqrt{gh}, & \text{for } kh \ll 1 \end{cases} \tag{17}$$

2.1.3. Nonlinear buoyancy and froude-Krylov wave excitation

Linear hydrodynamic models typically assume small-amplitude waves and body motions, which limits their ability to capture nonlinear effects. To account for weak nonlinearities, this study incorporates a method that computes buoyancy and Froude-Krylov forces based on the instantaneous submerged geometry and free surface elevation. Instead of relying solely on linear coefficients derived from potential flow solvers, the time-domain model evaluates static and dynamic pressures across the wetted surface panels at each time step, enabling more accurate representation of nonlinear wave-body interactions.

Wheeler stretching (Wheeler, 1969) is employed as a kinematic reconstruction technique in which the vertical coordinate is rescaled relative to the instantaneous free-surface elevation. This approach extends linear Airy wave kinematics above the mean water level by mapping the velocity field to the instantaneous surface elevation. It does not introduce nonlinear wave physics, but provides an approximate correction to improve velocity and pressure estimates near the free surface under finite wave amplitudes. The correction is performed using the transformation:

$$z^* = \frac{D(D + z)}{(D + \eta)} - D \tag{18}$$

where D represents the mean water depth, z is the original vertical coordinate of a point on the body, η is the instantaneous water surface elevation, and z^* is the corrected vertical coordinate after applying the Wheeler stretching method.

2.1.4. Viscous damping and Morison elements

To improve the accuracy of numerical simulations and align more closely with experimental observations, additional damping mechanisms can be introduced into the WEC-Sim model. This is particularly useful when (BEM)-based hydrodynamic coefficients do not fully capture the dissipative effects observed in real systems.

Viscous damping is incorporated using both linear and quadratic drag formulations. The resulting viscous force acting on a body can be expressed as:

$$F_v = -C_v\dot{X} - \frac{1}{2}C_d\rho A_d\dot{X}|\dot{X}| \tag{19}$$

$$= -C_v\dot{X} - C_D\dot{X}|\dot{X}|, \tag{20}$$

where C_v is the linear viscous damping coefficient, C_d is the dimensionless quadratic drag coefficient, ρ is the fluid density, and A_d represents the effective cross-sectional area subject to drag. The quadratic drag force term can also be defined more compactly using the coefficient C_D, which absorbs the constants and area term.

This approach provides greater flexibility for tuning the model to experimental data or observed field behavior, particularly in cases where flow separation and turbulence introduce nonlinear damping effects that are not captured by potential flow solvers.

2.2. Geometric design (MultiSurf)

MultiSurf was utilized to design the geometry of the platform. The platform is a standard barge platform, as depicted in Fig. 4. Following linear theory, only the wetted portion of the body was meshed in its undisplaced position using MultiSurf, resulting in a calculated draft of 4 m. The standard barge platform is modeled with 2240 rectangular panels that cover a quarter of the body. This barge has two geometric planes of symmetry with respect to the x-axis and y-axis, as shown in Fig. 4.

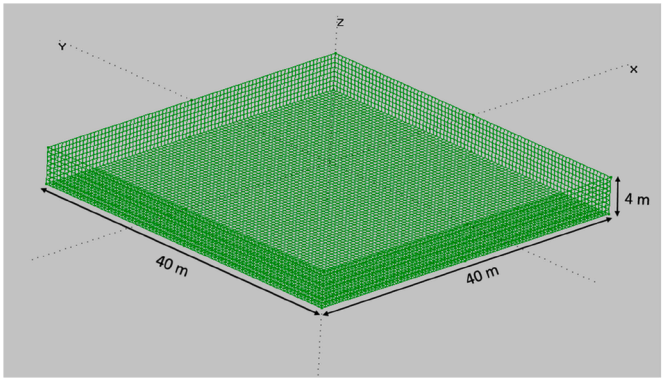

Fig. 4. Geometry of the standard barge platform.

2.3. Advanced hydrostatic and hydrodynamic calculations (WAMIT)

WAMIT was employed in this study to perform a frequency-domain analysis of the barge. The tool enabled the calculation of added mass, damping, and wave excitation forces across the surge, heave, pitch, and yaw degrees of freedom. These hydrodynamic coefficients provided important data for predicting the barge's response to regular and irregular waves and served as inputs for further time-domain simulations.

To characterize the frequency-dependent hydrodynamic behavior of the floating platform, the BEM solver WAMIT was used to compute the added mass $\mathbf{A}_{Hydro}(\omega)$, radiation damping $\mathbf{B}_{Hydro}(\omega)$, hydrostatic restoring matrix $\mathbf{C}_{Hydro}$, and wave excitation forces $f_{Hydro}(\omega)$. These outputs were generated based on the panel geometry defined in MultiSurf, enabling high-fidelity representation of the wetted surface.

The theoretical relationship between the added mass and damping terms is given by the complex potential formulation:

$$A_{ij} - \frac{i}{\omega} B_{ij} = \rho \iint_{S_b} n_i \varphi_j \, dS, \tag{21}$$

where φ_j is the velocity potential for mode j, n_i is the surface normal vector component in direction i, ρ is the fluid density, and S_b denotes the mean wetted surface.

For nondimensional analysis and scaling, normalized coefficients are computed as:

$$\bar{A}_{ij} = \frac{A_{ij}}{\rho L^k}, \tag{22}$$

$$\bar{B}_{ij} = \frac{B_{ij}}{\rho L^k \omega}, \tag{23}$$

where the scaling exponent k depends on the index pair (i, j) and relates to the nature of the corresponding hydrodynamic term: $k = 1$ for forces, $k = 2$ for moments, and higher values for mixed terms.

The hydrostatic properties of the platform are computed as surface integrals over the mean wetted surface S_b, employing Gauss' divergence theorem. The displaced volume is calculated from:

$$\forall = -\iint_{S_b} n_1 x \, dS = -\iint_{S_b} n_2 y \, dS = -\iint_{S_b} n_3 z \, dS, \tag{24}$$

and the coordinates of the center of buoyancy (x_b, y_b, z_b) are obtained from:

$$x_b = \frac{-1}{2\forall} \iint_{S_b} n_1 x^2 \, dS, \tag{25}$$

$$y_b = \frac{-1}{2\forall} \iint_{S_b} n_2 y^2 \, dS, \tag{26}$$

$$z_b = \frac{-1}{2\forall} \iint_{S_b} n_3 z^2 \, dS. \tag{27}$$

The matrix of hydrostatic and gravitational restoring coefficients is defined in Fig. 5.

$$C_{Hydro} = \begin{bmatrix} 0 & 0 & 0 & 0 & 0 & 0 \\ 0 & 0 & 0 & 0 & 0 & 0 \\ 0 & 0 & \rho g \iint_{S_b} n_3 \, dS & \rho g \iint_{S_b} y n_3 \, dS & -\rho g \iint_{S_b} x n_3 \, dS & 0 \\ 0 & 0 & 0 & \rho g \iint_{S_b} y^2 n_3 \, dS + \zeta & -\rho g \iint_{S_b} xy n_3 \, dS & \rho g \forall x_b + mg x_g \\ 0 & 0 & 0 & 0 & \rho g \iint_{S_b} x^2 n_3 \, dS + \zeta & -\rho g \forall y_b + mg y_g \\ 0 & 0 & 0 & 0 & 0 & 0 \end{bmatrix}$$

Fig. 5. Hydrodynamic matrix and gravitational restoring coefficients.

where (x_g, y_g, z_g) are the coordinates of the center of gravity of the system and $\zeta = \rho g \forall z_b - mgz_g$.

In this study, MOST was used to simulate the mooring forces on the floating barge under various environmental conditions. The mooring system was designed to provide sufficient restoring forces to counteract the platform's motion in surge, sway, and yaw. The quasi-static analysis ensured that the platform maintained its position and stability, even under significant wave and wind loading.

In the context of this study, MATLAB/Simulink was integrated with WECSim to simulate the overall dynamic response of the floating barge and its control systems.

In this work, Simulink was used to model the hybrid system of the NREL 5 MW wind turbine integrated into the platform along WECs. The aerodynamic and structural dynamics of the wind turbine were simulated, and a state-space controller was implemented to regulate the power output and rotor speed in turbulent wind conditions. Additionally, the results from the hydrodynamic analysis performed in WAMIT were integrated into Simulink for time-domain simulations of the barge's response under combined wind and wave loads.

The integration of WECSim, WAMIT, MOST, and MATLAB/Simulink provided a comprehensive simulation framework for analyzing the floating barge's performance, provided a flowchart in Fig. 6. The frequency-domain analysis from WAMIT was used to derive key hydrodynamic coefficients, which were then employed in the time-domain simulations in WECSim and Simulink. MOST ensured that the mooring forces were accurately modeled, contributing to the overall platform stability. This multi-tool approach allowed for detailed insights into the barge's dynamic behavior, energy extraction potential, and structural integrity under real-sea conditions.

3. Modeling results

3.1. Mass balance analysis

A critical initial step in the modeling process is verifying the mass balance of all components and ensuring the correct placement of the center of gravity. For a barge with a moonpool of 6000 m^3, the theoretical mass of displaced water is calculated as:

$$m = \rho V = 1025 \times 6000 = 6,150,000 \, \text{kg}. \tag{28}$$

The combined mass of all components in the system, based on Jonkman's thesis, is approximately $6,149,460$ kg, which introduces a negligible discrepancy of 540 kg. However, incorporating the downward force from the mooring system, estimated at $209,900$ kg, necessitates adjustments to the platform's mass distribution to maintain a draught of 4 m. The revised mass allocation ensures alignment with the required stability parameters.

The tower, as described by Jonkman, is positioned centrally within the moonpool and secured with a flat plate at the water level. In the ElastoDyn input file, the tower base height (`TowerBsHt`) is set to 0, representing its placement at the Mean Sea Level (MSL). Considering a freeboard height of 6 m, the total tower height from the barge deck becomes:

$$\text{Total Tower Height} = 87.6\,\text{m} - 6\,\text{m} = 81.6\,\text{m}. \tag{29}$$

This configuration ensures accurate modeling of the tower's structural parameters, including the center of mass and height relative to

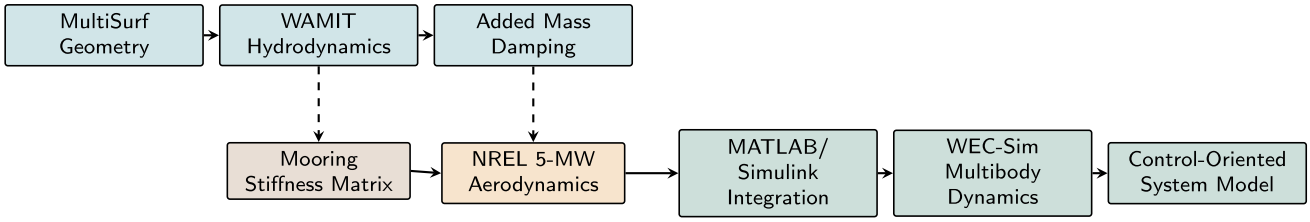

Fig. 6. Horizontal workflow of the coupled aero-hydro-servo simulation framework. Geometric and hydrodynamic preprocessing (MultiSurf, WAMIT) feed into parallel mooring and turbine dynamics modules, which integrate within MATLAB/Simulink via WEC-Sim multibody dynamics capabilities to generate the control-oriented platform model.

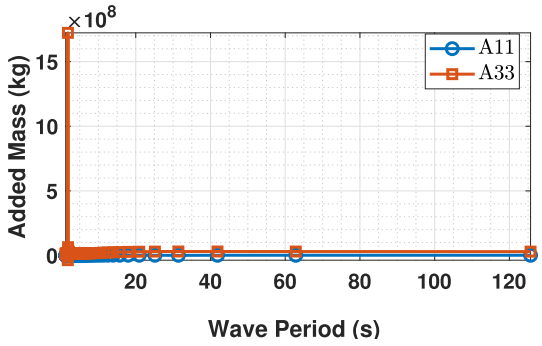

Fig. 7. Added mass coefficients for surge (A_{11}) and heave (A_{33}).

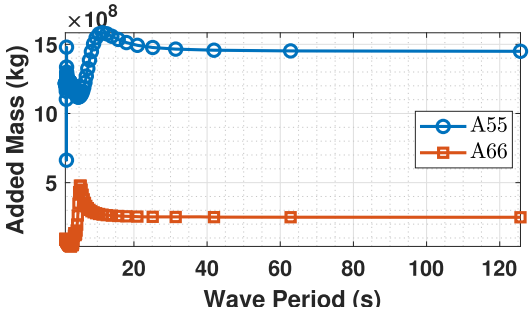

Fig. 8. Added mass coefficients for pitch (A_{55}) and yaw (A_{66}).

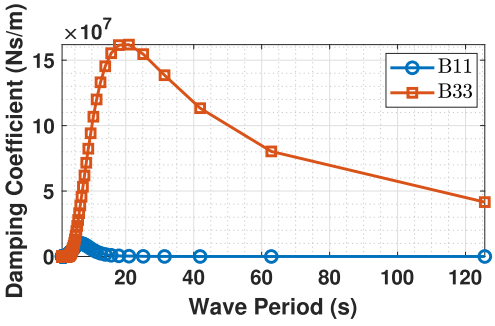

Fig. 9. Damping coefficients for surge (B_{11}) and heave (B_{33}).

the MSL. The hydrodynamic behavior of the barge was simulated using WAMIT to determine key hydrodynamic coefficients such as added mass, damping, and wave excitation forces. The calculations are centered at the barge's center of gravity to match Jonkman's baseline configuration, with simulations conducted under a range of wave frequencies. The hydrodynamic analysis of the floating barge equipped with an OWC was performed using WAMIT, a frequency-domain potential flow program. The focus of this analysis is to determine the added mass and damping coefficients, which are important in understanding the dynamic behavior of the structure when exposed to wave-induced forces. These coefficients play a significant role in predicting the response of the barge to wave excitations, as well as its stability and performance in offshore environments.

3.1.1. Added mass analysis

The added mass coefficients quantify the inertia effects due to the surrounding fluid acting on the floating barge. These coefficients change with varying wave frequencies and are calculated for different degrees of freedom: surge (A_{11}), heave (A_{33}), pitch (A_{55}), and yaw (A_{66}).

Fig. 7 illustrates the behavior of the added mass coefficients for surge (A_{11}) and heave (A_{33}) as a function of wave period. As expected, the added mass in surge remains relatively constant, showing that horizontal wave motions impart similar inertia effects across all frequencies. However, the heave added mass shows a prominent peak at shorter wave periods. This peak indicates significant interaction between the structure and the fluid in the vertical plane, particularly for higher frequency (short period) waves, which is characteristic of heave-dominated systems like floating barges.

In Fig. 8, the added mass coefficients for pitch (A_{55}) and yaw (A_{66}) are shown. Both pitch and yaw exhibit a higher added mass at lower wave periods, suggesting that the barge experiences greater rotational inertia due to the fluid at these frequencies. The results suggest that the platform's rotational response to waves will be more pronounced under short-period, high-frequency wave conditions, which should be taken into account when designing for stability.

3.1.2. Damping analysis

The radiation damping coefficients (B_{ij}) represent the energy dissipation due to wave radiation as the barge moves through the fluid. These coefficients are crucial in assessing the extent of energy loss during oscillations and play a significant role in understanding the barge's hydrodynamic performance under dynamic loads.

Fig. 9 presents the damping coefficients for surge (B_{11}) and heave (B_{33}). The damping in surge remains relatively small, implying limited energy dissipation in the horizontal direction. On the other hand, heave damping (B_{33}) shows a sharp increase at shorter wave periods, reaching a peak, which then decays as the period increases. This peak in heave damping is indicative of significant energy loss due to radiation, a behavior typical of floating platforms interacting with short, high-frequency waves in the vertical direction.

Similarly, Fig. 10 shows the radiation damping coefficients for pitch (B_{55}) and yaw (B_{66}). These coefficients reveal similar trends to the added mass, where significant energy dissipation is observed at shorter wave periods. This behavior suggests that the platform's rotational degrees of freedom (pitch and yaw) are sensitive to high-frequency waves, leading to more energy being radiated as wave-induced motion increases.

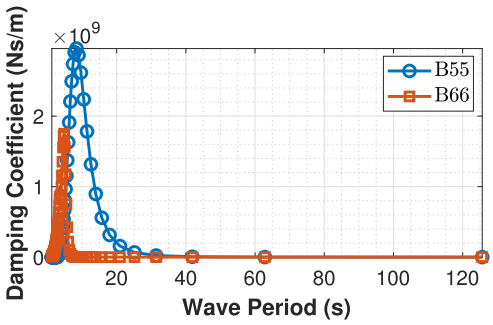

Fig. 10. Damping coefficients for pitch (B_{55}) and yaw (B_{66}).

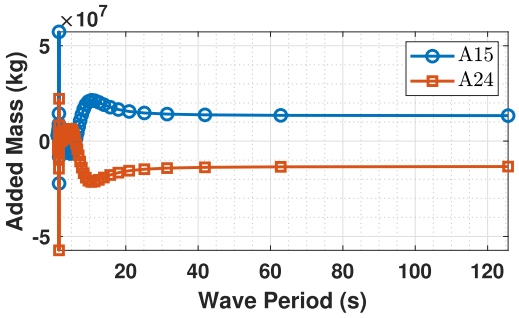

Fig. 11. Added mass coupling coefficients (A_{15}) and (A_{24}).

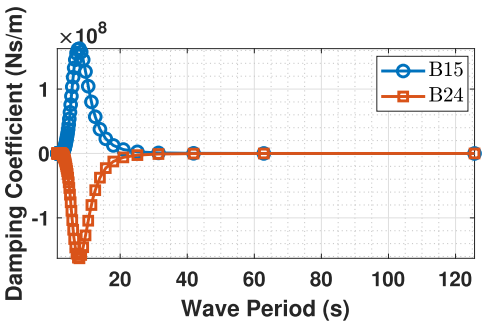

Fig. 12. Damping coupling coefficients (B_{15}) and (B_{24}).

3.1.3. Coupling terms

The coupling terms in the added mass and damping matrices reflect the interaction between different modes of motion, such as translation and rotation. These terms are essential in complex systems where significant cross-coupling can affect the overall dynamic response.

Figs. 11 and 12 show the added mass and damping coupling coefficients, respectively. The terms A_{15} and A_{24} represent coupling between translational and rotational motions in the surge-pitch and sway-roll planes, while B_{15} and B_{24} represent the corresponding damping terms. The results indicate non-zero values, particularly at shorter wave periods, signifying that these coupling effects must be considered when assessing the barge's dynamic stability and motion responses.

The WAMIT simulations provide key insights into the hydrodynamic characteristics of the barge with OWCs. The added mass and damping coefficients exhibit frequency-dependent behavior, with notable peaks at shorter wave periods, particularly in the heave, pitch, and yaw degrees of freedom. These trends reflect the increased interaction between the barge and surrounding water under high-frequency waves, leading to greater inertia and energy dissipation.

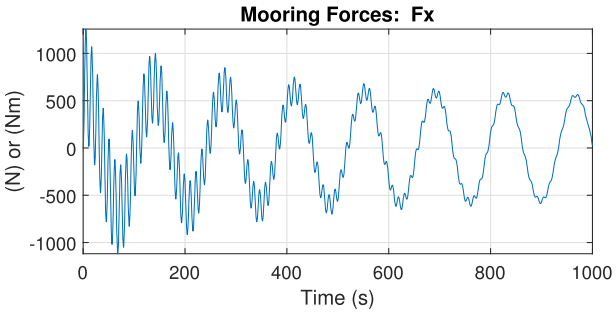

Fig. 13. Mooring system configuration for the NREL 5.0 MW offshore platform with the ITI Barge.

Table 2
Geometry and mass properties of the standard and OWC-Barge platforms.

Parameter	Value
Platform dimensions (W × L × H)	40 × 40 × 10 m
OWC chamber size (each)	5 × 5 × 10 m
Draft	4 m
Freeboard	6 m
Displacement (Standard Barge)	6400 m^3
Displacement (4-OWC Barge)	6000 m^3
Total mass (with ballast)	5.452×10^6 kg
Center of mass (below SWL)	0.2818 m
Roll inertia	7.27×10^8 kg m^2
Pitch inertia	7.27×10^8 kg m^2
Yaw inertia	1.45×10^9 kg m^2

In practical terms, these findings imply that the barge is highly responsive to short-period waves in both vertical and rotational motions. As a result, careful attention must be paid to the design and optimization of the platform's stability mechanisms, particularly its mooring system, to mitigate excessive motion and ensure operational efficiency under such conditions. Furthermore, the coupling effects between different degrees of freedom highlight the complex motion dynamics of the system. These effects can significantly impact the barge's overall behavior, particularly in mixed sea states where wave and wind loads interact across multiple axes.

3.2. Mooring system simulation

The mooring system is modeled using a catenary mooring system as mentioned in OpenFAST, which computes the quasi-static, non-linear mooring forces acting on the floating structure. The system accounts for surge, sway, and yaw motions, with the total mooring force aligned closely with previously validated OC4 systems. As shown in Fig. 13, the mooring system for the hybrid FOWT-OWC configuration ensures optimal platform stabilization under varying environmental conditions. The system consists of eight mooring lines, arranged symmetrically for stability. The mooring design optimizes platform station-keeping under dynamic ocean conditions, modeled in WEC-Sim.

The mooring system was designed and implemented using `MoorDyn v2` coupled with `WEC-Sim` to represent a symmetric eight-line catenary configuration providing restoring stiffness in surge, sway, and yaw directions. Each mooring line was modeled using a *chain-type* line element with a diameter of 0.08 m, a mass per unit length of 130.4 kg/m, and an axial stiffness (EA) of 5.89×10^8 N, ensuring sufficient tensile strength for station-keeping of the floating platform. A damping coefficient (BA) of -0.8 was specified, which `MoorDyn` internally converted into an equivalent viscous damping term. The normal drag and added mass coefficients were set to $C_d = 1.6$ and $C_a = 1.0$, respectively, while the tangential components were defined as $C_{d,ax} = 0.05$ and $C_{a,ax} = 0.0$, capturing hydrodynamic resistance effects along the line.

Table 3
Summary of MoorDyn input parameters used for the mooring system.

Parameter	Symbol / Value	Unit
Line type	Chain	–
Line diameter	$d = 0.08$	m
Mass per unit length	$m = 130.4$	kg/m
Axial stiffness	$EA = 5.89 \times 10^8$	N
Damping coefficient	$BA = -0.8$	–
Normal drag coefficient	$C_d = 1.6$	–
Tangential drag coefficient	$C_{d,ax} = 0.05$	–
Normal added mass coefficient	$C_a = 1.0$	–
Tangential added mass coefficient	$C_{a,ax} = 0.0$	–
Unstretched length per line	$L_0 = 473.312$	m
Number of segments	$N = 20$	–
Fairlead depth	$z = -4.0$	m
Anchor depth	$z = -150.0$	m
Water depth	$h = 150.0$	m
Bottom stiffness	$k_{bot} = 3.0 \times 10^4$	N/m
Bottom damping	$c_{bot} = 3.0 \times 10^5$	N·s/m
Integration time step	$\Delta t = 0.001$	s
Integrator type	2nd order Runge-Kutta	–

Table 4
Key Properties of the 5-MW NREL floating wind turbine.

Parameter	Value
Rotor diameter	126 m
Hub height	90 m
Tower mass	347 460 kg
Nacelle mass	240 000 kg
Hub mass	56 780 kg
Blade mass (each)	17 740 kg
Power rating	5 MW
Initial rotor speed	12.1 rpm
Wind speed (cut-in / rated / cut-out)	3/11.4/25 m s^{-1}
COG (tower)	38.2 m
Tower height	129.4 m
Generator efficiency	97%

The system geometry comprised 16 connection points, where each line connects between a body-mounted fairlead and a fixed seabed anchor point. The fairlead points were positioned around the floating body at a depth of −4.0 m in a symmetric square pattern with coordinates $(\pm 20, \pm 20, -4.0)$ m, while the anchor points were distributed correspondingly on the seabed at $(\pm 299.71, \pm 299.71, -150.0)$ m, consistent with a total water depth of 150 m. Each mooring line had an unstretched length of 473.312 m and was discretized into 20 segments for dynamic simulation. The coupled body was initialized at $(0, 0, -4.0)$ m

Static equilibrium was computed under calm-water conditions (no wave kinematics) using a second-order Runge-Kutta integrator with a time step of 0.001 s. Bottom stiffness and damping were defined as $k_{bot} = 3.0 \times 10^4$ N/m and $c_{bot} = 3.0 \times 10^5$ N·s/m, respectively, to avoid unrealistic seabed penetration. During the dynamic relaxation stage, the drag coefficients were scaled by a factor of 5.0 to accelerate convergence, with a threshold of 0.01 and a maximum iteration time of 200 s. The initialization converged successfully, yielding a static equilibrium suitable for dynamic simulations. The simulation outputs were configured to record the fairlead tension in each of the eight lines (`FairTen1-FairTen8`), enabling detailed post-processing of mooring loads and restoring characteristics. This configuration represents a balanced, horizontally symmetric catenary mooring system suitable for hybrid floating offshore wind-wave platforms, ensuring accurate coupling between platform hydrodynamics and mooring dynamics in `WEC-Sim`.

The geometry and mass properties of both the standard and OWC-barge platforms are summarized in Table 2, while the MoorDyn input parameters and the main properties of the 5-MW NREL floating wind turbine are given in Tables 3 and 4, respectively.

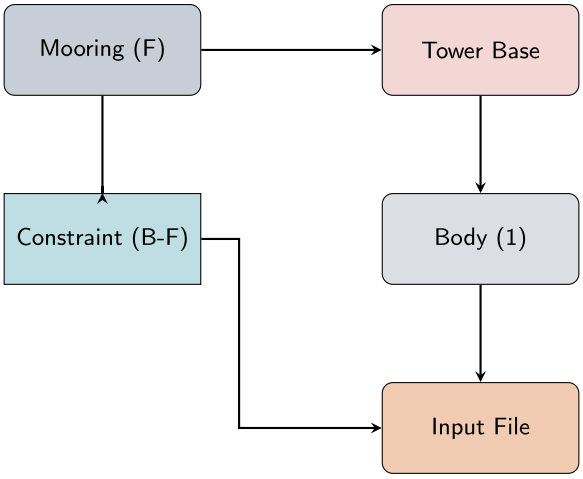

Fig. 14. Simulink flowchart representing the simulation framework of hybrid FOWT-OWC systems.

3.3. NREL 5 MW wind turbine integration

The dynamic response of the platform to wind forces is analyzed through the integration of a 5 MW NREL wind turbine as shown in Fig. 15. The output power and torque of the wind turbine can be expressed as:

$$P_w = \frac{1}{2} C_p(\vartheta, \lambda) \rho \pi r^2 v_{\text{wind}}^3 \tag{30}$$

$$Q_w = \frac{1}{2} C_Q(\vartheta, \lambda) \rho \pi r^2 v_{\text{wind}}^3 \tag{31}$$

where C_p and C_Q are the power and torque coefficients, respectively, ρ represents the air density (kg/m^3), and r denotes the rotor radius (m). The blade pitch angle is given by ϑ (in degrees), and the tip-speed ratio (TSR) λ is defined as:

$$\lambda = \frac{\Omega_t R}{v_{\text{wind}}} \tag{32}$$

Here, Ω_t is the rotational speed of the turbine in (rad/s), R is the rotor radius (m), and v_{wind} is the wind velocity (m/s). The power coefficient C_p is a nonlinear function of ϑ and λ and is expressed as:

$$C_p(\vartheta, \lambda) = 0.22\left(\frac{116}{\lambda_i} - 0.4\vartheta - 5\right) e^{-12.5/\lambda_i} \tag{33}$$

where:

$$\frac{1}{\lambda_i} = \frac{1}{\lambda + 0.087\vartheta} - \frac{0.035}{\vartheta^3 + 1} \tag{34}$$

The aerodynamic performance of the turbine is dictated by the interplay of these coefficients, which determine the energy capture efficiency. High-efficiency operation requires optimal alignment of the tip-speed ratio λ and blade pitch angle ϑ, ensuring maximum power extraction under varying wind speeds. Furthermore, the torque coefficient C_Q governs the mechanical dynamics, crucial for stable coupling with the generator. Advanced numerical techniques often calibrate these parameters to enhance turbine performance under real-world conditions. The simulation methodology is illustrated in Fig. 14, where the interaction between mooring, constraints, tower base, and input files is visualized. This structured representation facilitates the accurate modeling of dynamic responses within WEC-Sim simulink environment.

4. Dynamic response and results

4.1. Steady-state performance validation

A comparative assessment of steady-state turbine performance was conducted between the WEC-Sim-based hybrid model and OpenFAST

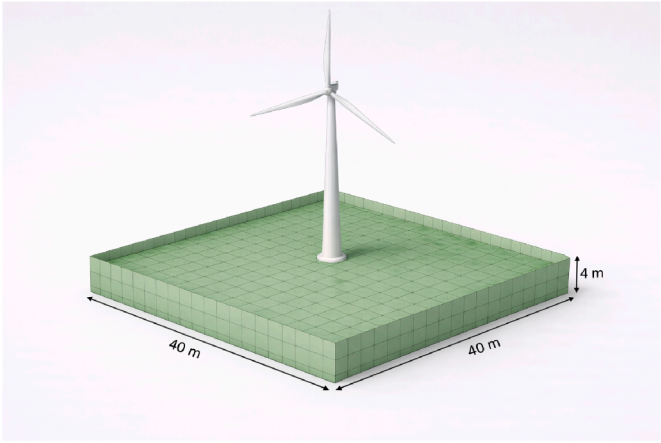

Fig. 15. WECSim model representation.

to validate the accuracy of the integrated aerodynamic and control system modules. Key operational variables, including rotor torque (kN·m), generator power (kW), and blade pitch angle (degrees), were evaluated across a wind speed range of 3-25 m/s, encompassing operating Regions 1, 2, and 3. The hybrid WEC-Sim model was developed entirely from scratch within a modular multibody framework, leveraging the Modular Open-Source Turbine (MOST) control implementation adapted to the NREL 5-MW reference turbine. The agreement with OpenFAST across all steady-state quantities substantiates the robustness of the WEC-Sim model for hybrid wind-wave platform simulations.

Fig. 16 shows the rotor torque profiles for both models. The WEC-Sim results closely match OpenFAST in Region 2 (approximately 5-11.4 m/s), following a quadratic trend characteristic of maximum power point tracking (MPPT). Both models reach a rated torque near 4300 kN·m at 11.4 m/s. The WEC-Sim torque continues to rise slightly to a peak of approximately 5300 kN·m by 12.1 m/s, reflecting a smoother transition into Region 3. This modest overprediction near the rated point remains within 20-25% and is likely attributable to minor implementation differences in generator damping or saturation handling. Generator power comparison in Fig. 17 further validates the aerodynamic consistency, with both models achieving a rated output of 5000 kW at the transition to Region 3. The deviation between WEC-Sim and OpenFAST is below 5% throughout Region 2, with the WEC-Sim output slightly lagging at 11 m/s due to conservative torque ramping, yet quickly converging to rated output beyond 12 m/s.

The blade pitch evolution, shown in Fig. 18, begins at 12 m/s in both models, consistent with the onset of Region 3. The WEC-Sim model exhibits a slightly steeper pitch increase, reaching 25.4° at 25 m/s compared to 23.1° in OpenFAST. This reflects a more responsive pitch control loop in the WEC-Sim implementation but retains stability throughout the high-wind operating regime. The close alignment across all steady-state metrics underscores the fidelity of the WEC-Sim control and aerodynamic modules. Importantly, the fully independent development of the WEC-Sim model, including the implementation of nonlinear rotor dynamics, torque-speed control, and blade pitch actuation, positions this framework as a strong candidate for future closed-loop control design, co-optimization studies, and hybrid offshore platform benchmarking.

The steady-state analysis demonstrates the effectiveness of the control strategies implemented and validations in both OpenFAST and WEC-Sim. The comparative study highlights the reliability of the hybrid FOWT-OWC model, providing a strong foundation for further control system development aimed at improving offshore renewable energy performance.

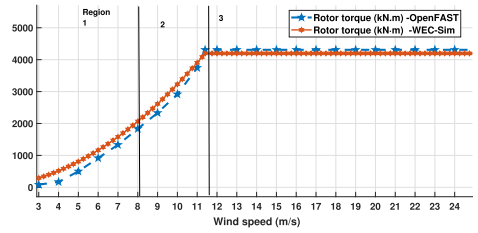

Fig. 16. Comparison of rotor torque versus wind speed between WEC-Sim and OpenFAST.

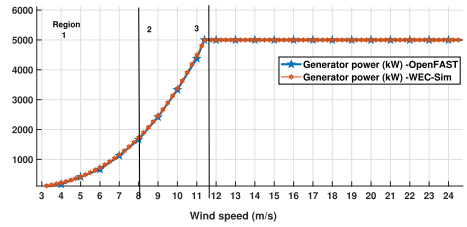

Fig. 17. Comparison of generator power versus wind speed between WEC-Sim and OpenFAST.

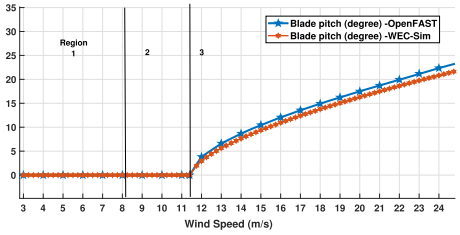

Fig. 18. Comparison of blade pitch angle versus wind speed between WEC-Sim and OpenFAST.

4.2. *Response amplitude operators (RAOs)*

The frequency-domain hydrodynamic characteristics of the hybrid FOWT-OWC platform were evaluated across all six rigid-body degrees of freedom, both with and without the wind turbine, to establish baseline system dynamics for control design (Figs. 19 and 20).

To verify model fidelity, response amplitude operators RAOs obtained from the first-principles WEC-Sim implementation were systematically compared with results from the industry-standard OpenFAST framework. The strong agreement confirms that the model accurately represents hydrostatic restoring effects, frequency-dependent added mass, and radiation damping-key hydrodynamic properties required for reliable control-oriented modeling of floating platforms.

The surge RAO demonstrates very close agreement between both tools across all wave periods examined. Both WECSim and OpenFAST predict a sharp resonance peak at approximately 12 s, with maximum surge amplitudes around 3.5 mm. The responses converge smoothly at longer wave periods, indicating consistent hydrodynamic damping characterization in both models.

Sway predictions reveal the smallest response amplitudes among the examined parameters, with peak values under 0.2 mm. The agreement between tools is very close, with both capturing the resonance behavior near 11 s. The relatively modest sway responses indicate effective lateral stability under the studied wave conditions.

Heave represents the most significant vertical response, reaching approximately 1 mm at resonance. Both models show nearly identical behavior, with response amplitudes gradually increasing through

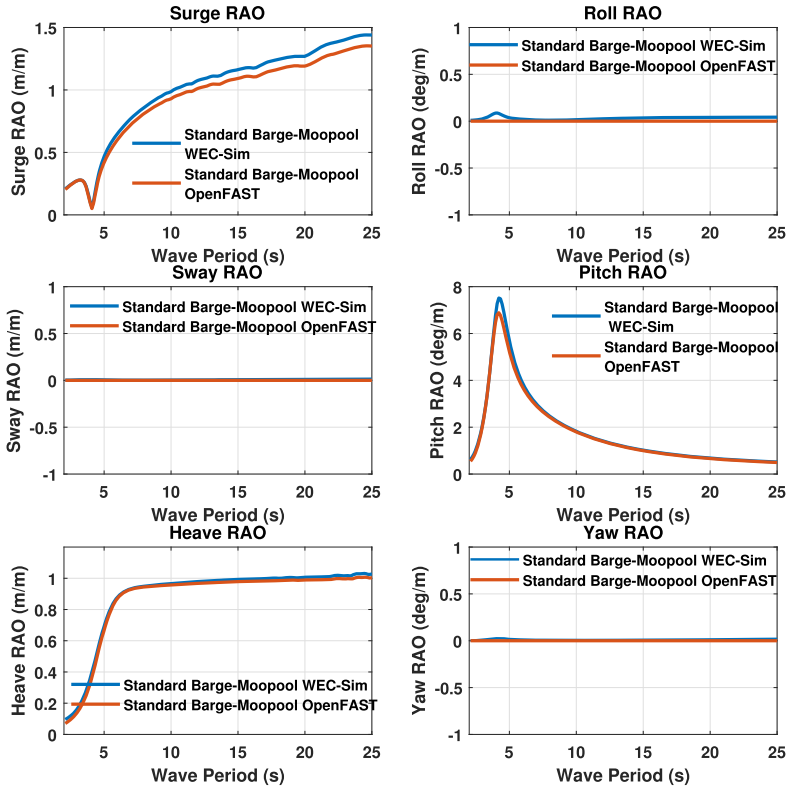

Fig. 19. Frequency-domain comparison of WECSim and OpenFAST response amplitude operators for all six platform rigid-body degrees of freedom without wind turbine integration.

Table 5
Free-decay derived dynamic parameters of the ITI barge.

DOF	Natural Period T_n (s)	δ	ζ
Surge	120	0.02	0.003
Heave	6.5	0.73	0.11
Pitch	10	0.22	0.035

mid-range wave periods and plateauing at longer wavelengths. This similarity suggests robust agreement in the vertical restoring force calculations. Pitch RAO peaks near 10 s at approximately 25 deg/m, representing the most energetic rotational response. WECSim predictions slightly exceed OpenFAST across the resonant range, though the general shape of the response curves aligns well. Yaw motions remain subdued throughout, with maximum amplitudes below 0.3 deg/m, consistent with the symmetric wave-vessel interaction geometry.

The comparison demonstrates a good quantitative agreement between WECSim and OpenFAST across the operationally relevant wave period spectrum ($T \in [5, 35]$ s). The normalized root-mean-square prediction differences remain below 3% in the resonance bands where platform dynamics are most pronounced. The WECSim model's incorporation of nonlinear multibody effects and the coupled feedback of the integrated OWC system results in marginally higher resonant amplitudes compared to the linearized OpenFAST approximation, reflecting enhanced physical fidelity. This validated model now provides a reliable computational foundation for subsequent controller synthesis, real-time simulation, tuning, and experimental verification studies.

The analysis reveals that WECSim and OpenFAST generally produce consistent RAO predictions, validating the WECSim modeling for the feedback and control applications.

The analysis reveals that WECSim and OpenFAST generally produce consistent RAO predictions, validating the WECSim modeling for the feedback and control applications.

4.3. Free decay response analysis

The free decay response tests were conducted to evaluate the natural periods and damping characteristics of the ITI barge integrated with the NREL 5 MW wind turbine model. These tests were performed for surge, heave, and pitch motions under no-wave and no-wind conditions. However, specific adjustments were required to overcome the limitations of the MOST framework to ensure accurate and reliable results.

The free decay response in surge (see in Fig. 21) motion revealed a natural period of approximately 134.22 s, corresponding to a frequency of 0.0075 Hz. This value aligns well with the previously reported data on the NREL forum for similar configurations. The response curve demonstrated the expected long-period oscillations, indicating the platform's low-frequency behavior in the horizontal plane.

For heave motion (see in Fig. 22), the natural period was determined to be 7.56 s, equivalent to a frequency of 0.1323 Hz. The heave response exhibited rapid damping, consistent with the hydrodynamic forces acting in the vertical plane. This behavior is crucial for understanding the platform's response to wave-induced forces.

The pitch motion analysis yielded a natural period of 11.38 s, corresponding to a frequency of 0.0879 Hz (see in Fig. 23). This result closely matches the NREL-reported value of 0.0863 Hz. The pitch decay

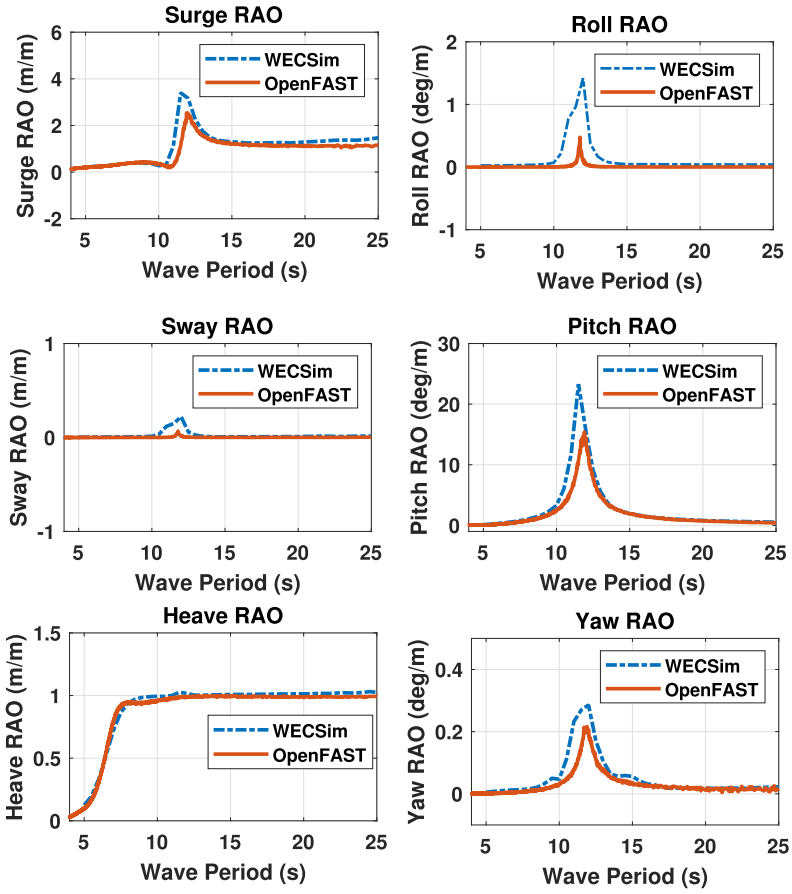

Fig. 20. Frequency-domain comparison of WECSim and OpenFAST response amplitude operators for all six platform rigid-body degrees of freedom. WECSim predictions (dashed blue lines) exhibit good agreement with OpenFAST reference solutions (dashed red lines) across the operationally relevant spectrum, validating the hydrodynamic and structural representation implemented in the first-principles model. (For interpretation of the references to colour in this figure legend, the reader is referred to the web version of this article.)

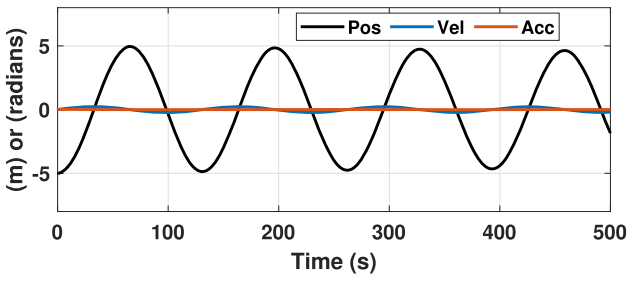

Fig. 21. Surge response of the ITI barge showing position, velocity, and acceleration over time.

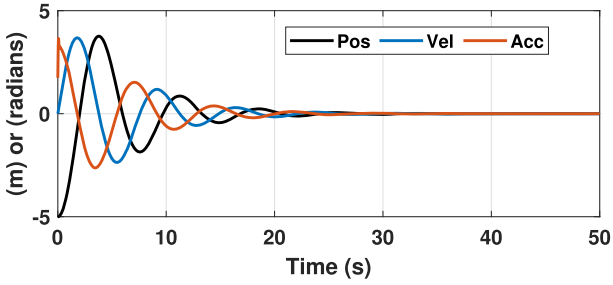

Fig. 22. Heave response of the ITI barge showing position, velocity, and acceleration over time.

curve highlighted the platform's energy dissipation in rotational motion, with progressively damping oscillations over time. The numerical results from these tests validate the model's dynamic behavior, demonstrating consistency with theoretical predictions and experimental data. Therefore, free decay response curves provide key insights into the system's stability, making them a crucial point for future optimization of offshore floating platforms.

These numerical results validate the model's dynamic behavior and are consistent with theoretical predictions. The analysis provides critical insights into the platform's stability and damping characteristics, aiding in the design and optimization of floating offshore systems.

For lightly damped oscillatory motion, the logarithmic decrement δ is computed from successive peak amplitudes:

$$\delta = \ln\left(\frac{x_i}{x_{i+1}}\right) \tag{35}$$

The damping ratio ζ is then obtained as:

$$\zeta = \frac{\delta}{\sqrt{(2\pi)^2 + \delta^2}} \tag{36}$$

The equivalent linear damping coefficient can be expressed as:

$$c_{\text{eq}} = 2\zeta\sqrt{km} \tag{37}$$

Table 6
Comparative analysis of WEC-Sim and OpenFAST model results.

Parameter	WEC-Sim Result	OpenFAST Result	Technical Significance
Natural Period (Surge)	134.22 s (0.0075 Hz)	Previously reported data	Validates low-frequency surge response for barge-type platforms, consistent with theoretical predictions.
Natural Period (Heave)	7.56 s (0.1323 Hz)	Matches NREL data	Confirms vertical plane dynamics and damping characteristics essential for platform operability.
Natural Period (Pitch)	11.38 s (0.0879 Hz)	Matches NREL data	Matches well with NREL value of 0.0863 Hz, verifying accurate pitch dynamics.
Rated Rotor Torque	~4300 kN·m (peak ~5300 kN·m)	~4300 kN·m	Slight overprediction near rated wind speed indicates a smoother transition into Region 3, attributable to nonlinear control implementation.
Rated Generator Power	5000 kW	5000 kW	Consistent rated power output with deviation below 5 percent across Region 2 validates aerodynamic and control logic.
Blade Pitch at 25 m/s	25.4°	23.1°	Indicates stronger pitch actuation in WEC-Sim, suggesting effective control performance under high wind loading.
Peak Pitch RAO	~23 deg/m at ~12 s	~15 deg/m at ~12 s	Higher resonance peak in WEC-Sim reflects nonlinear effects and dynamic feedback from the OWC, absent in linearized models.
Peak Heave RAO	~1.05 m/m at ~12 s	~1.05 m/m at ~12 s	good agreement demonstrates reliable modeling of vertical wave excitation effects.
Peak Surge RAO	~2.9 m/m at ~12.5 s	~3.0 m/m at ~12.5 s	good match in surge motion confirms fidelity in wave force modeling and horizontal dynamics.

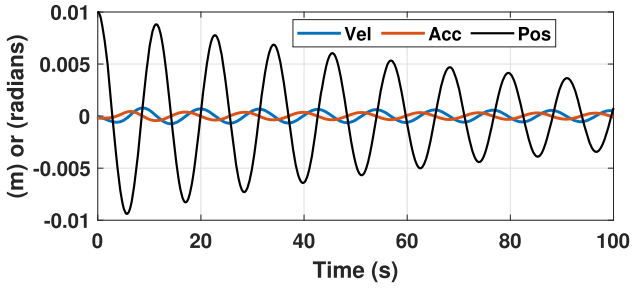

Fig. 23. Pitch response of the ITI barge showing position, velocity, and acceleration over time.

where m is the generalized mass and k is the hydrostatic restoring stiffness.

The free-decay results reveal distinct damping characteristics (see Table (5)) across modes. Surge exhibits extremely low damping, indicating minimal horizontal energy dissipation dominated by mooring stiffness. Heave shows moderate damping ($\zeta \approx 0.11$), reflecting significant radiation damping and viscous effects. Pitch presents light damping ($\zeta \approx 0.035$), consistent with hydrostatic restoring dominance and limited viscous moment dissipation.

5. Validation and comparative assessment of nonlinear hybrid platform dynamics

This study has developed and validated a comprehensive non-linear WEC-Sim model tailored for hybrid floating offshore wind platforms that integrate WECs devices. The model extends the capabilities of existing simulation tools by offering a multibody, control-oriented framework capable of capturing coupled aero-hydro-elastic dynamics with high fidelity. Implemented in MATLAB/Simulink using the WEC-Sim environment and Simscape Multibody solver, this model facilitates the simulation and control design of hybrid platforms operating in realistic offshore conditions.

A key distinguishing feature of the developed model is its fully nonlinear treatment of platform dynamics, in contrast to the linearized approximations employed in conventional tools such as OpenFAST. By integrating hydrodynamic coefficients from WAMIT, aerodynamic and structural data from the NREL 5-MW reference turbine via MOST, and a quasi-static mooring system, the model accurately replicates the coupled physical behavior of the hybrid system. Direct comparisons with OpenFAST outputs across multiple operational regions demonstrate similar behavior in key performance indicators such as rotor torque, generator power, and platform motion responses.

The analysis of Response Amplitude Operators highlights the damping effect of the OWC on pitch motions, offering a promising strategy for enhancing platform stability under wave excitation. This insight addresses a critical challenge in floating offshore wind technology by leveraging the inherent dynamics of the OWC for passive stabilization.

Table 6 presents a detailed technical comparison between the WEC-Sim model and the OpenFAST benchmark, demonstrating the precision, innovation, and value of the model for advanced control development and optimization at the system level.

These results confirm the robustness and reliability of the nonlinear WEC-Sim model in simulating hybrid offshore platforms. The model offers an accurate and versatile simulation environment suitable for advancing research in active control strategies, energy harvesting optimization, and the design of future floating renewable systems. Its integration of OWC damping and nonlinear dynamic fidelity positions it as a valuable tool for both academic investigation and industry applications.

6. Code and data availability

The complete simulation framework developed in this study is publicly available to support transparency, reproducibility, and future control-oriented research. The repository can be accessed via Zenodo at: https://doi.org/10.5281/zenodo.18772113

The archived dataset includes the platform geometry the MultiSurf files, hydrodynamic database generated with WAMIT, the MATLAB/WEC-Sim simulation environment, and the validation scripts used for free-decay tests, RAO analysis, and OpenFAST comparisons. In addition, representative output datasets and plotting routines are provided to facilitate verification and post-processing.

The framework has been tested with MATLAB R2024a or later and WEC-Sim v6.0 or newer. Installation requires approximately 15 min on a standard workstation, and a typical 500 s nonlinear time-domain simulation completes in approximately 10 min, depending on hardware configuration.

7. Limitations and future validation requirements

This study presents numerical verification only. Model fidelity cannot be confirmed without experimental measurements. Critical uncertainties requiring experimental calibration include:

1. **Viscous drag coefficients**: We assume $C_d = 0.6$ for the platform bottom and $C_d = 1.0$ for vertical members, based on literature values. Actual coefficients depend on Reynolds number and surface roughness. Uncertainty: ±30%.
2. **PTOs analysis**: While energy extraction is not the focus at this stage, the intent is to enable future implementation of active feedback control strategies based on OWC-inspired damping mechanisms. In future extensions, full two-phase OWC modeling, dynamic air chamber pressure effects, and PTO control architectures will be incorporated to explore co-optimization of energy conversion and platform stability.
3. **Aerodynamic-platform coupling at high angles**: BEM theory assumes small platform pitch angles (< 10°). Beyond this range, blade inflow angles become skewed.
4. **OWC chamber hydrodynamics**: WAMIT computes linear potential flow solutions. Viscous losses at chamber openings and sloshing modes are not captured.

   Experimental verification: The present study does not include experimental validation. Experimental validation is identified as an important direction for future work. Scale model testing (1:50) is planned in collaboration with ACG Labs. Until experimental validation is complete, **this model should be considered a numerical benchmark for control algorithm development, not a design tool for physical systems.**

8. Conclusions

This study presented a control-oriented nonlinear benchmark framework for floating offshore wind turbines incorporating oscillating water column chambers, developed to address structural limitations in existing aero-hydro-servo-elastic simulation tools that restrict direct state access for feedback control synthesis. Rather than proposing new physical formulations, the work focused on the architectural design of a transparent simulation environment in which all subsystem states, coupling forces, and nonlinear interactions are synchronously accessible for control analysis.

The framework integrates first-principles aerodynamic modeling, geometry with MultiSurf, WAMIT-derived radiation-diffraction hydrodynamics, nonlinear Froude-Krylov and viscous drag forces, quasi-static catenary mooring dynamics, and servo-drivetrain coupling within WEC-Sim's multibody formulation in MATLAB/Simulink. This architecture enables direct access to the full six-degree-of-freedom platform state vector at each solver step, eliminating asynchronous control delays inherent in DLL-based interfaces and supporting multivariable feedback design under large-amplitude platform motion.

Model verification was conducted through free-decay tests, hydrodynamic response analysis, and cross-platform comparison with OpenFAST. The free-decay analysis confirmed natural periods and damping characteristics consistent with hydrostatic predictions and radiation damping behavior, while RAO analysis identified resonance frequencies aligned with published ITI barge data.

The primary contribution of this work lies in the establishment of a reproducible, control-enabling benchmark model that supports stability analysis, gain-scheduled control design, and robustness evaluation under coupled wind-wave excitation. The framework provides a platform for systematic investigation of platform pitch stabilization, load mitigation, and hybrid wind-wave co-design strategies that are difficult to implement feedback control in order to mitigate the undesired motion for the platform stability.

Future work will extend the framework to include OWC air-chamber thermodynamics, turbine power take-off dynamics, and active damping control, enabling integrated aero-hydro-pneumatic control strategies. Experimental validation and hardware-in-the-loop implementation will further support the transition from high-fidelity simulation to field-deployable control solutions for hybrid offshore energy platforms.

CRediT authorship contribution statement

Irfan Ahmad: Conceptualization, Data curation, Formal analysis, Investigation, Methodology, Writing – original draft; **Nataliia Sergiienko:** Conceptualization, Data curation, Validation, Writing – review & editing; **Aitor J. Garrido:** Conceptualization, Funding acquisition, Investigation, Methodology, Supervision, Writing – review & editing; **Izaskun Garrido:** Conceptualization, Data curation, Funding acquisition, Investigation, Supervision, Validation, Writing – review & editing.

Declaration of competing interest

The authors declare that they have no known competing financial interests or personal relationships that could have appeared to influence the work reported in this paper.

Acknowledgment

The authors would like to thank the Basque Government and UPV/EHU for partially funding their research work through Grant IT2006-26. The authors also acknowledge funding from MICIU/AEI/10.13039/501100011033 and FEDER, UE through projects PID2021-123543OB-C21 and PID2024-155653OB-C22, as well as support through UPV/EHU-grant POSTUPV25/02.

References

Aboutalebi, P., Garrido, I., Nguyen, D. T., & Garrido, A. J. (2026). Stabilization and dynamic control of semi-submersible hybrid floating wind turbine–oscillating water column platforms. *Energy Conversion and Management*, *348*(Part A), 120623. https://doi.org/10.1016/j.enconman.2025.120623

Aboutalebi, P., M'zoughi, F., Garrido, I., & Garrido, A. (2021). Performance analysis on the use of oscillating water column in barge-based floating offshore wind turbines. *Mathematics*, *9*(3), 246. https://doi.org/10.3390/math9030246

Ahmad, F., M'zoughi, F., Aboutalebi, P., & Garrido, I. (2023a). Fuzzy logic control of an artificial neural network-based floating offshore wind turbine model integrated with four oscillating water columns. *Ocean Engineering*, *272*, 112599. https://doi.org/10.1016/j.oceaneng.2023.112599

Ahmad, I., M'zoughi, F., Aboutalebi, P., Garrido, I., & Garrido, A. J. (2023b). Fuzzy logic control of an artificial neural network-based floating offshore wind turbine model integrated with four oscillating water columns. *Ocean Engineering*, *269*, 113578. https://doi.org/10.1016/j.oceaneng.2022.113578

Ahmad, I., M'zoughi, F., Aboutalebi, P., Garrido, I., & Garrido, A. J. (2023c). A regressive machine-learning approach to the non-linear complex FAST model for hybrid floating offshore wind turbines with integrated oscillating water columns. *Scientific Reports*, *13*, 1499. https://doi.org/10.1038/s41598-023-28703-z

Ahmad, I., Neshat, M., Garrido, A., & Garrido, I. (2025). Optimization of control-oriented AI models for real-time platform pitch prediction in hybrid wind-wave offshore systems. *Energy Reports*, *14*, 2670–2687. https://doi.org/10.1016/j.egyr.2025.09.006

Aslmostafa, E., Mirzaei, M. J., Hamida, M. A., & Plestan, F. (2026). Experimental evaluation of robust nonlinear control strategies for regions II and III for floating offshore wind turbines. *Ocean Engineering*. *346*, 123887. https://doi.org/10.1016/j.oceaneng.2025.123887

Aubault, A., Alves, M., & Sarmento, A. (2011). Modeling of an oscillating water column on the floating foundation windfloat. *Journal of Offshore Mechanics and Arctic Engineering*, *133*(2), 021401. https://doi.org/10.1115/1.4002706

Bai, D., Wang, B., Li, Y., & Wang, W. (2025). Study on load reduction and vibration control strategies for semi-submersible offshore wind turbines. *Scientific Reports*, *15*, 1148. https://doi.org/10.1038/s41598-025-85476-3

Chandrasekaran, C., & Sricharan, V. (2021). Numerical study of bean-float wave energy converter with float number parameterization using WEC-sim in regular waves with the levelized cost of electricity. *Ocean Engineering*, *236*, 109504. https://doi.org/10.1016/j.oceaneng.2021.109504

Chen, S., Xie, P., Liao, J., & Huang, Z. (2024). Experimental model studies on active hardstand compensation control strategy for offshore wind turbine installation vessels. *Ocean Engineering*. https://doi.org/10.1016/j.oceaneng.2024.116789

Drew, B., Plummer, A. R., & Sahinkaya, M. N. (2009). A review of wave energy converter technology. *Proceedings of the Institution of Mechanical Engineers, Part A: Journal of Power and Energy*, *223*(8), 887–902.

European Commission (2023). Revised Renewable Energy Directive. Technical Report European Union.

Fu, J., Shi, W., Han, X., Karimirad, M., Wang, T., & Li, X. (2025). Development and performance study of a multi-degree-of-freedom loading device for real-time hybrid model testing of floating wind turbines. *Marine Structures*, *99*, 103717. https://doi.org/10.1016/j.marstruc.2024.103717

Fu, S., Jin, Y., Zheng, Y., & Chamorro, L. P. (2019). Wake and power fluctuations of a model wind turbine subjected to pitch and roll oscillations. *Applied Energy*, *253*, 113605. https://doi.org/10.1016/j.apenergy.2019.113605

Gu, X., Lin, F., Jiang, W., Xu, J., Liu, J., Wang, K., & Tao, T. (2025). Power efficiency and dynamic characteristics of a 15 MW floating wind turbine with wave energy conversion concept. *Horizons*, *13*, 100125. https://doi.org/10.1016/j.horiz.2024.100125

Hassan, A., Ahmad, G., Shafiullah, M., & Islam, A. (2025). Review of intelligent frameworks for pitch angle control in wind turbines. *IEEE Access*. https://doi.org/10.1109/ACCESS.2025.10345678

He, S., Wang, B., & Chen, Y. (2025). Improved optimal torque control for large-scale floating offshore wind turbines via interval type-2 fuzzy logic system. *Ocean Engineering*, *330*, 121186. https://doi.org/10.1016/j.oceaneng.2025.121186

Industry Research (2024). Offshore Wind Market - Growth, Trends, and Forecasts (2024 - 2025). Technical Report Global Market Insights.

Kung, S.-Y., Arun, K. S., & Rao, D. V. B. (1983). State-space and singular-value decomposition-based approximation methods for the harmonic retrieval problem. *JOSA*, *73*(12), 1799–1811.

Lin, C., Zhang, Q., Sheng, S., Zhou, B., Xiang, R., Wu, X., Zhou, Z., & Jin, P. (2025). Novel design and performance evaluation of a hybrid system of floating offshore wind turbine and sharp-eagle WECs. *Ocean Engineering*, *340*, 122387. https://doi.org/10.1016/j.oceaneng.2025.122387

M'zoughi, F., Bouallegue, S., Garrido, A. J., Garrido, I., & Ayadi, M. (2018). Programmed fuzzy gain scheduling of PI-based airflow control for an oscillating water column in wave power generation plants. *IEEE Journal of Oceanic Engineering*, *44*(4), 1058–1076.

M'zoughi, F., Bouallegue, S., Garrido, A. J., Garrido, I., & Ayadi, M. (2020). Airflow control in the water cycle for oscillating water column energy converters. *Proceedings of the Institution of Mechanical Engineers, Part I Journal of Systems and Control Engineering*, *234*(1), 118–133.

Pereira, R. D. O., Ríos, C. S. N., & Moreira, J. P. R. (2024). Active structural control of floating offshore wind turbine based on PID controller and resonance filter. In *Ieee energy conference*. https://doi.org/10.1109/ENERGYCON.2024.10407038

Rafia, H., Ouadi, H., Giri, F., & Boulal, A. (2026). Multi-objective control of floating offshore wind turbines in region III: Reference optimization and adaptive regulation based on artificial neural networks. *Ocean Engineering*. *343*(Part 5), 123382. https://doi.org/10.1016/j.oceaneng.2025.123382

Sarkar, S., & Fitzgerald, B. (2020). Vibration control of spar-type floating offshore wind turbine towers using a tuned mass-damper-inerter. *Structural Control and Health Monitoring*, *27*(1), e2471. https://doi.org/10.1002/stc.2471

Sebastian, B., Karmakar, D., & Rao, M. (2024). Coupled dynamic analysis of semi-submersible floating wind turbine integrated with oscillating water column WEC. *Ocean Engineering and Marine Energy*, *10*, 345-359. https://doi.org/10.1007/s40722-024-00212-5

Sergiienko, N. Y., Xue, L., da Silva, L. S. P., Ding, B., & Cazzolato, B. S. (2025). Statistical analysis of floating hybrid wind-wave energy systems. *Applied Energy*, *401*, 126669. https://doi.org/10.1016/j.apenergy.2025.126669

Shittu, A. A., Machado, G. S., Zhang, J., Shadman, M., & Estefen, S. F. (2025). Reliability assessment of a hybrid floating wind turbine concept based on coupled aero-hydro-structural dynamics. *Journal of Ocean Engineering and Marine Energy*, *11*, 1007–1026. https://doi.org/10.1007/s40722-025-00416-7

Song, H., Yu, T., Tong, X., Zhao, X., Zhang, Z., Lun, Z., Wang, L., & Wang, Z. (2026). Hybrid offshore wind and wave energy systems: A review. *Energies*, *19*(3), 739. https://doi.org/10.3390/en19030739

Tang, S., Cai, W., Fang, J., & Qiao, Y. (2026a). Individual pitch control for platform–rotor coupled dynamics stabilization in floating offshore wind turbines. *Ocean Engineering*, *349*, 124194. https://doi.org/10.1016/j.oceaneng.2026.124194

Tang, Y., Chen, M., Yuan, Z., Jiang, X., Yu, N., Li, T., & Choo, Y. S. (2026b). Advancing floating offshore wind turbine construction from the perspective of wet towing using a tugboat with autonomous control. *Marine Structures*, *107*, 103973. https://doi.org/10.1016/j.marstruc.2025.103973

U. S. Department of Energy (2024). Offshore Wind Market Report: 2024 Edition. Technical Report Office of Energy Efficiency & Renewable Energy.

Wang, W., Li, H., Sheng, K., Chen, L., Wang, Y., Yang, Y., & Wang, Y. (2026). Cooperative motion control of ATMD and gyrostabilizer for floating wind turbines based on model predictive control. *Ocean Engineering*, *343*(Part 2), 123190. https://doi.org/10.1016/j.oceaneng.2025.123190

Wei, Z., Borthwick, A. G. L., Cao, F., Zhao, C., Han, M., Tao, J., & Shi, H. (2025). Power performance of an offshore floating hybrid wind and wave energy converter. *Energy Conversion and Management*, *341*, 120023. https://doi.org/10.1016/j.enconman.2025.120023

Wheeler, J. D. (1969). Method for calculating forces produced by irregular waves. *Journal of Waterways and Harbors Division*, *95*(1), 33–52.

Wind Energy Insights (2024). Global Offshore Wind Market Outlook to 2029. Technical Report Renewable Energy Analytics.

WindEurope (2024). Offshore Wind in Europe: Key trends and statistics 2024. Technical Report WindEurope.

Xie, W., Lu, Y., Liang, H., He, Y., Zhang, Z., Jin, Z., & Tian, H. (2025). Experimental analysis of intelligent vibration control structures for offshore wind turbine towers based on real-time hybrid simulation. *Structures*, *61*, 106097. https://doi.org/10.1016/j.istruc.2024.106097

Yi, Y., Sun, K., Liu, Y., Zhang, J., Zhang, H., Zhu, R., & Yao, H.-D. (2026). Coupled numerical framework for wind-wave-to-wire energy conversion in floating hybrid wind-wave systems. *Applied Energy*, *403*, 127106. https://doi.org/10.1016/j.apenergy.2025.127106

Zhai, Y., Li, X., Wang, C. M., & Wang, W. (2025). Experimental study on dynamic response of floating offshore wind turbine integrated with aquaculture cage. *Renewable Energy*, *219*, 119457. https://doi.org/10.1016/j.renene.2025.119457

Zhang, D., Chen, Z., Liu, X., Sun, J., Yu, H., & Zeng, W. (2022). A coupled numerical framework for hybrid floating offshore wind turbine and oscillating water column wave energy converters. *Energy Conversion and Management*, *256*, 115340. https://doi.org/10.1016/j.enconman.2022.115340

Zhang, H., Liu, X., Cao, X., Zhang, N., & Law, A. W. K. (2025). Dynamic response and power performance of a novel wave energy system with single-point mooring integration. *Energy*, *325*, 136114. https://doi.org/10.1016/j.energy.2025.136114